New Journal of Physics
The open access journal at the forefront of physics

Deutsche Physikalische Gesellschaft DPG
IOP Institute of Physics

Published in partnership with: Deutsche Physikalische Gesellschaft and the Institute of Physics

OPEN ACCESS

RECEIVED
15 March 2022

REVISED
23 August 2022

ACCEPTED FOR PUBLICATION
27 September 2022

PUBLISHED
27 October 2022

PAPER

Polarized photoelectrons from converging vector waves

B Hafizi[1,*], D Younis[2] and D F Gordon[1]

[1] Naval Research Laboratory, Washington, DC 20375, United States of America
[2] Department of Physics and Astronomy, University of Rochester, Rochester, NY 14627, United States of America
[*] Author to whom any correspondence should be addressed.

E-mail: bahman.hafizi@nrl.navy.mil, dan.younis@outlook.com and daniel.gordon@nrl.navy.mil

Keywords: spin polarization, photoionization, structured light

Supplementary material for this article is available online

Abstract

This paper investigates the spin characteristics of photoelectrons when hydrogen-like ions are centro-symmetrically irradiated with converging vector waves—a non-paraxial form of structured light. For a photon with given total angular momentum and third component thereof, photoelectrons with both helicities are obtained—in contrast to the fixed helicities produced by left- or right-circularly polarized light. The angular distribution of photoelectrons is broadly tunable through the radiation mode numbers, and opposite helicities can be extracted in synchronism.

1. Introduction

The search for new forces, particles, symmetries or extra dimensions is optimized by employing polarized electrons and positrons in linear colliders [1]. With the wide-spread availability of sources of intense electromagnetic radiation, the possibility of generating polarized leptons by laser beams is under investigation.

Most analyses of photoionization are restricted to plane wave irradiation, sometimes with paraxial corrections. The analysis herein breaks from this paradigm by computing the electronic wavefunction under illumination by spherical waves in the near field, where no paraxial representation of the field is possible. The geometry is illustrated in figure 1 (see methods for details). This configuration imposes practical difficulties, such as producing a coherent, converging, spherical wave of a given wavelength, and positioning an atom with wavelength-scale precision. If these difficulties prove insurmountable, this work nevertheless provides a building-block for analysis of related configurations.

The specific spherical waves considered are the electromagnetic multipole fields [2]. These modes play a special role in spin couplings, because, unlike Bessel and Laguerre–Gauss beams, they are the exact eigenfunctions of the total angular momentum operator and its projection. It is important in this regard to distinguish between the near and far field. In the far field, multipole modes consist of both inward and outward propagating components, which are globally eikonal and locally paraxial. If an atom is placed in the far field, it experiences only the local paraxial field, with locally approximate quantum numbers, and the results are similar to what one obtains from existing analyses. In the near field, the atom experiences the full set of angular momentum quantum numbers that define the mode, and the results are very different.

An example of one of the low-order multipoles is shown in figure 1. Some aspects of the structure can be described in the language of vector beams [3]. On the other hand, there are observation points where the wavevector is orthogonal to the angular momentum projection. This characteristic is more reminiscent of spatio-temporal optical vortices [4].

Early investigations of the interaction with electrons (e.g. Thomson/Compton scattering) include those in references [5, 6]. One of the findings of these is that there is a mass change, proportional to the intensity, induced in the electron due its quiver motion which in turn results in a shift of the frequency of the scattered photon.

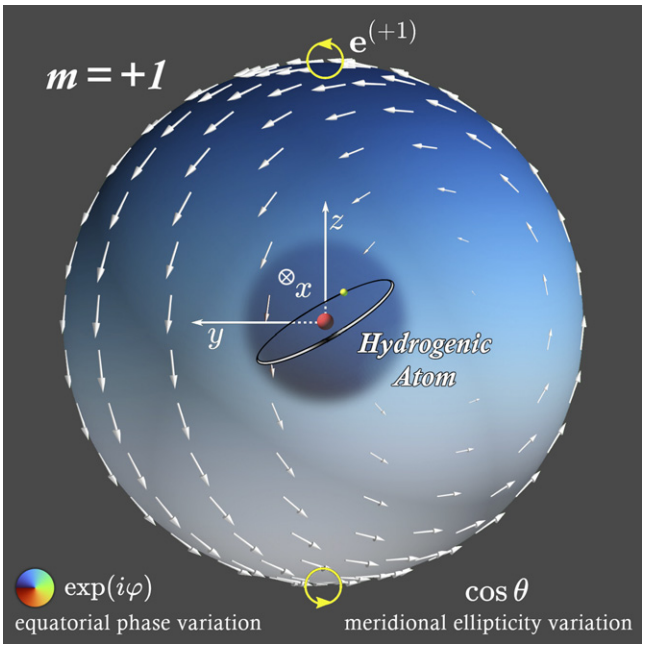

Figure 1. Poincaré sphere for a spherical wave of magnetic photons, classified as $M1$ radiation, with total angular momentum $j = 1$ and $m = +1$ component thereof. The arrows indicate the electric field at a given instant in time. Photons observed at the poles are in pure helicity states $\mathbf{e}^{(+1)} = -\mathrm{i}(\mathbf{e}_x + \mathrm{i}\mathbf{e}_y)/\sqrt{2}$ (appearing as left-circularly-polarized looking towards the incoming wave). Photons observed on the equator are linearly polarized, but have a phase variation $x + \mathrm{i}y \propto \mathrm{e}^{+\mathrm{i}\varphi}$. Photons observed on the meridian are in-phase, but have an ellipticity variation. This paper analyzes a hydrogenic atom in the ground state, at the center of the system.

The photon's polarization is imprinted on the polarization of the reaction products. A detailed analysis of the spin of the byproducts in the Bethe–Heitler process $Z + \gamma \to Z + e^- + e^+$ was given in reference [7]. Helicity transfer in Coulomb scattering of leptons was analyzed in reference [8]. The influence of the photon spin in single-photon ionization was discussed in reference [9]. In another context, it has been shown that the spin of a lepton flips in magnetic bremsstrahlung [10]. This relatively slow process is in use in storage rings to generate polarized beams.

Studies of polarization characteristics in QED processes expanded with advances in high-intensity laser technology, typically considering circularly polarized photons [11–22]. 'Twisted' light, having definite polarization and projection of orbital angular momentum (e.g. Bessel beams), has been employed to provide a picture of the transitions that can be excited between atomic states, to determine the distribution of photoelectrons and, using that distribution, to characterize energy circulation within Bessel beams [23–27] (see also reference [28]). Generation of polarized electrons in a semiconductor using twisted photons is discussed in [29].

Production of polarized electrons using circularly-polarized light in the multiphoton regime was analyzed in reference [30] and subsequent experiments with Xe atoms showed two peaks, corresponding to opposite spin polarizations, owing to the dependence of the ionization probability on the magnetic quantum number of the orbitals [31]. This dependence has been exploited to produce a spin-polarized relativistic beam by ionization injection of electrons into a beam-driven plasma wakefield [32]. This relies on the magnetic quantum number dependence of strong-field ionization of the $5p^6$ electron of Xe atoms and the subsequent trapping and acceleration of the photoelectrons in Li plasma.

This paper considers a light source distinct from any of those noted above. To motivate this, note that the transversality requirement $k^\mu e_\mu = 0$ (k^μ is the photon four-momentum and e_μ is the unit polarization four-vector) of electromagnetic fields and the fact that the photon is massless mean that the spin $\hat{\mathbf{s}}$ and the orbital angular momentum $\hat{\mathbf{l}}$ are not distinguishable—only the total angular momentum $\hat{\mathbf{j}} = \hat{\mathbf{l}} + \hat{\mathbf{s}}$ has physical meaning [33], whence it is possible to consider photons with definite *total angular momentum*. In particular, the photon's vector wavefunction $\mathbf{A}$ is assumed to satisfy

$$\hat{\mathbf{j}}^2\mathbf{A} = j(j+1)\mathbf{A} \qquad (1)$$

$$\hat{j}_z\mathbf{A} = m\mathbf{A}$$

i.e. it is the simultaneous eigenvector of the squared total angular momentum operator and of its projection in a specified direction. The form of equation (1) immediately suggests that $\mathbf{A} \propto \mathbf{Y}_{jm}$ where $\mathbf{Y}_{jm}$ is a vector spherical harmonic with eigenvalues j and m $(= -j, -j+1, \ldots, j-1, j)$, respectively.

Vector spherical waves [2, 33, 34] break up into two classes, electric 2^j-pole (Ej) photons and magnetic 2^j-pole (Mj) photons. Magnetic photons are characterized by the vanishing of the radial component of the electric field. The defining condition $\mathbf{r} \cdot \mathbf{E}_{jm}(\mathbf{r}) = \mathbf{r} \cdot \mathbf{A}_{jm}(\mathbf{r}) = 0$ makes them analogous to TE modes of straight, cylindrical waveguides [2]. All the non-vanishing field components can be expressed in terms of the radial component of the magnetic field. Electric photons, on the other hand, have no radial component of magnetic field, in analogy with TM modes.

The spherical unit vectors $\mathbf{e}^{(\pm 1)} \equiv \mp \mathrm{i}(\mathbf{e}_x \pm \mathrm{i}\mathbf{e}_y)/\sqrt{2}$, $\mathbf{e}^{(0)} \equiv \mathrm{i}\mathbf{e}_z$ are conveniently used to express the components of the spherical harmonic vectors. For light described by $\hat{\mathbf{e}}^{(+1)}$ the projection of the *angular* momentum on the z-axis is positive and this defines a positive helicity state. Correspondingly, $\hat{\mathbf{e}}^{(-1)}$ defines a negative helicity state.

Spherical waves of photons live in a space built up from a non-separable product of the orbital and spin vector spaces—formally, a tensor product. The state of polarization of these waves (i.e. the proportion of orbital angular momentum and spin) can be mapped onto a Poincaré sphere. This representation is a powerful tool for visualization of the resultant vectors (methods & figure 1). The discussion here centers on the polarization characteristics of the electrons photoionized by spherical waves of photons. The vector potential $A^{\mu}(x)$ belongs to the class of vector fields which, as noted above, are specified by their angular momentum rather than their linear momentum. Use is made of the lowest order S-matrix element [33, 35, 36]

$$S_{fi} \equiv \langle f|S^{(1)}|i\rangle = -\mathrm{i}e \int \mathrm{d}^4x \bar{\psi}_f(x)\, \gamma_\mu A^\mu(x) \psi_i(x) \quad (f \neq i), \tag{2}$$

where e (<0) is the charge on an electron, $\psi_i(x)$ and $\psi_f(x)$ are the initial (bound) and final (photoelectron) states, both of which are solutions of the Dirac equation (standard notation for Dirac matrices γ^μ is employed). The spinor electrodynamics keeps track of all relevant terms, both in the bound state and in the outgoing state, to ensure validity of the results for $Z\alpha < 1$ (i.e. the analysis is not limited to low Z), as well as applicability for photoionization with high-energy (MeV-class) photons. The range of atomic numbers and photon energies considered is relevant to a variant of the Bethe–Heitler process for generation of polarized electron–positron pairs using spherical waves.

One possible source for processes requiring MeV-class photons (e.g. pair creation by the Bethe–Heitler mechanism) is the gamma quanta from radionuclides, which are naturally emitted in the form of overlapping Ej and Mj multipoles, covering the keV–MeV energy range. The flux from these sources is limited by the quantity available. The photons from the intense lasers available with present-day technology are in the infrared and cannot directly drive such processes. However, there are several approaches whereby these lasers can be used for generation of photons with energies in the MeV range and with high flux. An example of this is nonlinear Compton scattering process $e + n\omega \rightarrow e' + \gamma$ wherein an electron can absorb multiple photons and then emit a high-energy one [37–42]. Simulations of the interaction of laser radiation with tailored plasma indicate that this along with magnetic bremsstrahlung are two processes responsible for generation of high-energy photons covering the range from sub-MeV to ∼1 GeV [43–48]. One can thus envisage the availability of high-energy photons for processes such as photoionization and pair creation. These sources have a broad spectral range and do not share all the characteristics associated with laser light.

The ionization rate is computed by forming $|S_{fi}|^2$, integrating over appropriate variables and—if the polarization of the photoelectron were not of interest—summing over the spins of the final state as well. However, since the polarization of the photoelectron is of *primary* interest here, the last step is bypassed. Instead, the operator

$$\Sigma(s) = \frac{1}{2}(1 - \gamma_5 \not{s}), \tag{3}$$

formed from the matrix four-pseudovector $\gamma_5\gamma^\mu$ and the four-pseudovector s may be used to project out the *final* state with spin vector s_μ (satisfying $s^\mu p_\mu = 0$). (Equation (3) applies to electrons as well as to positrons.) Averaging over the *initial* spin states must be carried out as usual. Equation (3) is employed to examine the photoelectron polarization as the polarization state of the ionizing photons varies on the Poincaré sphere.

Coupling of electrons with magnetic photons is specially interesting. Taking the nonrelativistic limit momentarily, the photon's wavefunction couples to the electron current through the magnetic moment operator

$$\hat{\boldsymbol{\mu}} = \frac{e}{2mc}\hat{\mathbf{l}} + \frac{\mu}{s}\hat{\mathbf{s}},$$

where $\mu/s = -|e|\hbar/mc$ relates the magnetic moment μ and the spin s for an electron (exclusive of radiative correction). This expression is a linear combination of the orbital and the spin angular momenta. In the process of photoionization there is a specific proportion of helicity that an electron carries off according to its direction of ejection and, in turn, this is determined by the proportion of orbital angular momentum and helicity of the incident photon.

2. Methods

2.1. Spherical waves of photons & the Poincaré sphere

The spherical harmonic functions provide a unitary transformation from angular momentum representation to angular coordinate representation. In the case of *Ej* radiation, the vector potential $A^\mu = (\Phi(\mathbf{r}, t), \mathbf{0})$ reduces to a scalar potential [33]

$$\Phi(\mathbf{k}) \equiv -\sqrt{\frac{j+1}{j}}\frac{4\pi^2}{\omega^{3/2}}\delta(|\mathbf{k}| - \omega)Y_{jm}(\hat{\mathbf{k}})$$

for the wavefunction of photons with unit propagation vector $\hat{\mathbf{k}} = \mathbf{k}/\omega$, total angular momentum j and azimuthal component indexed by m. Fourier expansion of the form $\Phi(\mathbf{k}, t) \equiv \Phi(\mathbf{k})\mathrm{e}^{-\mathrm{i}\omega t}$ is assumed throughout.

For *Mj* radiation, $A^\mu = (0, \mathbf{A}(\mathbf{r}, t))$ where [2, 33]

$$\mathbf{A}_{jm\omega}(\mathbf{k}) \equiv \frac{4\pi^2}{\omega^{3/2}}\delta(|\mathbf{k}| - \omega)\mathbf{Y}^{(m)}_{jm}(\hat{\mathbf{k}}). \tag{4}$$

The magnetic spherical harmonic vector $\mathbf{Y}^{(m)}_{jm}(\hat{\mathbf{k}})$—identified by the superscript (m)—is expressible in terms of the scalar spherical harmonic $Y_{jm}(\theta_{\hat{\mathbf{k}}}, \varphi_{\hat{\mathbf{k}}})$

$$\mathbf{Y}^{(m)}_{jm}(\hat{\mathbf{k}}) = \frac{1}{\sqrt{j(j+1)}}\hat{\mathbf{k}} \times \nabla_{\hat{\mathbf{k}}} Y_{jm}(\theta_{\hat{\mathbf{k}}}, \varphi_{\hat{\mathbf{k}}}),$$

where $\nabla_{\hat{\mathbf{k}}} \equiv \left[\partial/\partial\theta_{\hat{\mathbf{k}}}, (1/\sin\theta_{\hat{\mathbf{k}}})\partial/\partial\varphi_{\hat{\mathbf{k}}}\right]$ and $\theta_{\hat{\mathbf{k}}}$, $\varphi_{\hat{\mathbf{k}}}$ denote the polar angle and the azimuth of $\hat{\mathbf{k}}$ relative to fixed axes *xyz*. The two-element gradient operator $\nabla_{\hat{\mathbf{k}}}$ acts on functions that depend solely on the direction of $\hat{\mathbf{k}}$.

Acting with the inversion operator on the *polar* vector in equation (4)

$$\hat{p}\mathbf{Y}^{(m)}_{jm}(\hat{\mathbf{k}}) = \frac{-1}{\sqrt{j(j+1)}}(-\hat{\mathbf{k}}) \times (-\nabla_{\hat{\mathbf{k}}})Y_{jm}(\theta_{\hat{\mathbf{k}}} - \pi, \varphi_{\hat{\mathbf{k}}} + \pi) = (-1)^{j+1}\mathbf{Y}^{(m)}_{jm}(\hat{\mathbf{k}})$$

whence the parity of the magnetic photons is $(-1)^{j+1}$. Note that the total angular momentum states are normalized according to

$$\int \frac{\mathrm{d}^3k}{(2\pi)^4}\omega\omega' \mathbf{A}^*_{j'm'\omega'}(\mathbf{k})\cdot\mathbf{A}_{jm\omega}(\mathbf{k}) = \omega\,\delta(\omega' - \omega)\delta_{jj'}\delta_{mm'}.$$

In coordinate representation the spherical wave covers the entire space and thus in equation (4), ω (and $\mathbf{k}$) is a continuous variable.

Making use of equation (4), the field representation in *xyz*-space is

$$\mathbf{A}_{jm\omega}(\mathbf{r}) = \int \frac{\mathrm{d}^3k}{(2\pi)^3}\,\mathrm{e}^{\mathrm{i}\mathbf{k}\cdot\mathbf{r}}\mathbf{A}_{jm\omega}(\mathbf{k}) = \frac{2\mathrm{i}^j\sqrt{\omega}\,g_j(kr)}{\sqrt{j(j+1)}}\mathbf{r} \times \nabla Y_{jm}(\mathbf{r}/r), \tag{5}$$

where $g_j(kr) = \sqrt{\pi/2kr}\,J_{j+1/2}(kr)$ is a spherical Bessel function. Equation (5) may be rewritten as

$$\mathbf{A}_{jm\omega}(\mathbf{r}) = \frac{2\mathrm{i}^j\omega^{j+1/2}}{\sqrt{j(j+1)}}\frac{g_j(kr)}{(kr)^j}\mathbf{r} \times \nabla[r^j Y_{jm}(\mathbf{r}/r)], \tag{6}$$

where $r^j Y_{jm}(\mathbf{r}/r)$ is a rank j spherical tensor with $2j+1$ components. For the case of $M1$ radiation (i.e. $j = 1$, $m = -1, 0, +1$) one finds

$$\sqrt{\frac{4\pi}{3}}\nabla[rY_{1,-1}(\mathbf{r}/r)] = \frac{\mathrm{i}}{\sqrt{2}}(\mathbf{e}_x - \mathrm{i}\mathbf{e}_y) \equiv \mathbf{e}^{(-1)}$$
$$\sqrt{\frac{4\pi}{3}}\nabla[rY_{1,0}(\mathbf{r}/r)] = \mathrm{i}\mathbf{e}_z \equiv \mathbf{e}^{(0)} \tag{7}$$
$$\sqrt{\frac{4\pi}{3}}\nabla[rY_{1,+1}(\mathbf{r}/r)] = -\frac{\mathrm{i}}{\sqrt{2}}(\mathbf{e}_x + \mathrm{i}\mathbf{e}_y) \equiv \mathbf{e}^{(+1)},$$

where the last equalities relate the *spherical unit vectors* $\mathbf{e}^{(-1)}$, $\mathbf{e}^{(0)}$, $\mathbf{e}^{(+1)}$ to the Cartesian ones. The pair $\mathbf{e}^{(+1)}$ and $\mathbf{e}^{(-1)}$ constitute the *photon* helicity eigenvectors $\mathrm{i}\mathbf{e}_z \times \mathbf{e}^{(\lambda)} = \lambda\mathbf{e}^{(\lambda)}$ with eigenvalues $\lambda = +1$, $\lambda = -1$, respectively. In the helicity bases

$$\mathbf{A}_{1,m\omega}(\mathbf{r}) = \sqrt{\frac{3}{2\pi}}\omega^{3/2}\frac{g_1(kr)}{kr}\begin{cases} -z\mathbf{e}^{(-1)} + \dfrac{1}{\sqrt{2}}(x - \mathrm{i}y)\mathbf{e}^{(0)} & m = -1 \\ \dfrac{1}{\sqrt{2}}[(x - \mathrm{i}y)\mathbf{e}^{(+1)} + (x + \mathrm{i}y)\mathbf{e}^{(-1)}] & m = 0 \\ z\mathbf{e}^{(+1)} + \dfrac{1}{\sqrt{2}}(x + \mathrm{i}y)\mathbf{e}^{(0)} & m = +1. \end{cases} \tag{8}$$

The Stokes parameter $S_0 = |\mathbf{A}_{jm\omega}(\mathbf{r})|^2$ is related to the intensity (Poynting flux) [2]. As an example, for $j = 1$,

$$S_0 = \frac{3}{2\pi}\omega^3\left[\frac{g_1(kr)}{kr}\right]^2\begin{cases} z^2 + \dfrac{1}{2}(x^2 + y^2) & m = -1 \\ x^2 + y^2 & m = 0 \\ z^2 + \dfrac{1}{2}(x^2 + y^2) & m = +1. \end{cases} \tag{9}$$

The significance of equation (8) is made apparent by using $x \pm \mathrm{i}y = \sqrt{x^2 + y^2}\,\mathrm{e}^{\pm\mathrm{i}\varphi}$. The $M1$ photon is seen to comprise an admixture of states carrying $\pm\hbar$ units of *orbital* angular momentum along with $\pm\hbar$ units *helicity* associated with the unit vectors. On the z axis, the photon is in a pure helicity state; in the x–y plane it carries one unit ($\mathrm{e}^{\pm\mathrm{i}\varphi}$) of orbital angular momentum and no helicity.

The vector fields considered here are very different from the Laguerre–Gaussian eigenmodes [49–56]. Typically, a laser beam is elliptically-polarized in the x–y plane—and remains so along the propagation direction z. For circularly-polarized light travelling in the z-direction, the electric and magnetic fields are [2]

$$\mathbf{E}(\mathbf{r}, t) \approx \left[E_0(x, y, t)\mathbf{e}^{(\pm 1)} + \frac{1}{k}\left(\frac{\partial E_0}{\partial x} \pm \mathrm{i}\frac{\partial E_0}{\partial y}\right)\mathbf{e}^{(0)}\right]\mathrm{e}^{\mathrm{i}(kz - \omega t)},$$
$$\mathbf{B}(\mathbf{r}, t) \approx \mp\mathrm{i}\sqrt{\mu\epsilon}\,\mathbf{E}(\mathbf{r}, t).$$

where $E_0(x, y, t)$ is the slowly-varying complex-valued envelope. Equation (8), on the other hand, represents a field that is *structured* in its intensity, phase, polarization, and orbital angular momentum—so-called fully structured light—with spatially-varying angular momentum states. These characteristics are displayed on the Poincaré sphere as in figure 1. Vector field generation by employing a polarization optic in a laser cavity has been reported in reference [57].

2.2. *S*-matrix element, ionization rate & helicity

Rather than spin, it is helicity—i.e. the component of spin along the direction of velocity—that is useful because it commutes with the Hamiltonian and is a 'good' quantum number. Equation (3) serves as the operator of interest in studies of lepton polarization. Helicity states describe longitudinally-polarized leptons which are eigenstates of the operator in equation (3), numbering two in total.

In the ultra-relativistic limit, the polarization operator goes over to $\frac{1}{2}(1 \pm \gamma_5)$ for electrons and $\frac{1}{2}(1 \mp \gamma_5)$ for positrons. In the standard representation, with $\mathbb{1}_2$ standing for the 2×2 unit matrix, the chirality operator takes the form

$$\gamma_5 \equiv -\mathrm{i}\gamma^0\gamma^1\gamma^2\gamma^3 = \begin{pmatrix} 0 & -\mathbb{1}_2 \\ -\mathbb{1}_2 & 0 \end{pmatrix}.$$

The sign convention here conforms to that in reference [33], which is opposite to that in some references (e.g. references [35, 58]).

For the vector potential in equation (6), the relevant component of the electron current density four-vector is $\boldsymbol{j}_{fi} = \psi_f^\dagger(\mathbf{r})\boldsymbol{\alpha}\psi_i(\mathbf{r})\mathrm{e}^{-\mathrm{i}(E_g - \varepsilon)t}$ for transitions from initial state i to final state f (supplementary

sections 1–3). The polarization of the initial state can be up or down with equal probability. As far as the final state is concerned, one often sums over their polarizations [33, 35, 59–61]. Here, however, it is the polarization of the photoelectron that is of interest and the summation is not performed.

For photons having definite values of j, m, equation (2) leads to the differential ionization rate [33]

$$\mathrm{d}w_{jm} = 2\pi\delta(\varepsilon - E_g - \omega)|(V_{fi})_{jm}|^2\mathrm{d}\nu,$$

where $(V_{fi})_{jm} \equiv C\bar{u}_f(p,s)Au_i(\uparrow\downarrow)$, $u_i(\uparrow\downarrow)$ and $\bar{u}_f(p,s)$ are the initial (bound) and final (photoelectron) states; these, along with expressions for C and A, are given in supplementary sections 1–3.

When a photon with definite *angular momentum* causes an electron to transition from a bound state into a final state belonging to the continuous spectrum, $\mathrm{d}\nu \to \mathrm{d}\omega\,\mathrm{d}^3p/(2\pi)^3$ and integration over frequency leads to

$$\mathrm{d}w_{jm} = |(V_{fi})_{jm}|^2\Big|_{\omega=\varepsilon-m+I} \times \frac{\varepsilon p\,\mathrm{d}\varepsilon\,\mathrm{d}\Omega_p}{(2\pi)^2} \tag{10}$$

in which $\mathrm{d}\Omega_p = \mathrm{d}(\cos\theta_p)\mathrm{d}\varphi_p$ is the element of solid angle wherein the photoelectron lies, and (θ_p, φ_p) are the polar and azimuthal angles of the electron.

The final form of the expression for the ionization rate is obtained after taking into account the spin of the electron. If the polarization of the initial electron is not known and that of the final electron is not measured, the ionization rate reduces to the oft-used summation [35]

$$\frac{1}{2}\sum_{\uparrow\downarrow,s}|\bar{u}(p,s)Au(\uparrow\downarrow)|^2 \tag{11}$$

which can be simplified by employing the usual trace formulae [33, 35].

The goal here is to go beyond equation (11) and determine how the polarization of the photons controls that of the emerging photoelectrons. To do so, use is made of the expression for the polarization density matrix $\rho = \frac{1}{2}(\not{p} + m)(1 - \gamma_5 \not{s})$ [33, 35]. This reduces to $\rho(\uparrow\downarrow) = m(\gamma^0 + 1)/2$ for the (unpolarized) ground state. For the photoelectron, $\rho = \frac{1}{2}(\gamma^0\varepsilon - \boldsymbol{\gamma}\cdot\mathbf{p} + m)(1 - \gamma_5 \not{s})$ and equation (11) goes over into the trace

$$\frac{m}{4}\,\mathrm{Tr}\big[(\gamma^0\varepsilon - \boldsymbol{\gamma}\cdot\mathbf{p} + m)(1 - \gamma_5 \not{s})A(\gamma^0 + 1)\bar{A}\big]. \tag{12}$$

The degree of polarization

$$P(\mathbf{p}) \equiv \frac{N^{(+1/2)}(\mathbf{p}) - N^{(-1/2)}(\mathbf{p})}{N^{(+1/2)}(\mathbf{p}) + N^{(-1/2)}(\mathbf{p})}$$

is the ratio of the difference $N^{(+1/2)}(\mathbf{p}) - N^{(-1/2)}(\mathbf{p})$ in the number of photoelectrons with the two possible helicities divided by the total number. For $|P(\mathbf{p})| \to 0$ the two polarizations are equally likely; $|P(\mathbf{p})| \to 1$ is of particular interest herein. Making use of equation (12) for electron helicity states $\lambda = +1/2$ and $\lambda = -1/2$ in the ultra-relativistic limit, the degree of polarization is [reference [33], equation (29.22)]

$$P(\mathbf{p}) \approx \frac{\mathrm{Tr}\big[(\gamma^0\varepsilon - \boldsymbol{\gamma}\cdot\mathbf{p})\gamma_5 A(\gamma^0 + 1)\bar{A}\big]}{\mathrm{Tr}\big[(\gamma^0\varepsilon - \boldsymbol{\gamma}\cdot\mathbf{p})A(\gamma^0 + 1)\bar{A}\big]}. \tag{13}$$

Moreover, using equation (10) one finds

$$w_{jm} = \frac{e^2(mZe^2)^5}{2j(j+1)\pi^3}\int \mathrm{d}\Omega_p \int_{m-I}^{\infty}\mathrm{d}\varepsilon p\,\frac{\mathrm{Tr}\big[(\gamma^0\varepsilon - \boldsymbol{\gamma}\cdot\mathbf{p} + m)A(\gamma^0 + 1)\bar{A}\big]}{(\varepsilon - m + I)^3} \tag{14}$$

for the total ionization rate for the given incident power level.

Using the trace theorems, it can be shown that in the limit of plane wave irradiation the analysis here goes over to that in section 58 of reference [33]. For spherical waves, the integration over the azimuthal angle of the photons can be performed analytically, the integration over the polar angle and the trace evaluations in equations (13) and (14) are performed numerically (supplementary section 3).

3. Results

The formalism presented applies to both types of photons—be they electric or magnetic. In light of the closing paragraph of section 1, and for brevity, consideration will henceforth be limited to magnetic photons.

Consider the case of photoionization of hydrogen-like xenon ion Xe^{53+}. In the analysis presented here, the approximation $Z\alpha < 1$ is made at several points (supplementary sections 1–3); Xe^{53+} fulfils this

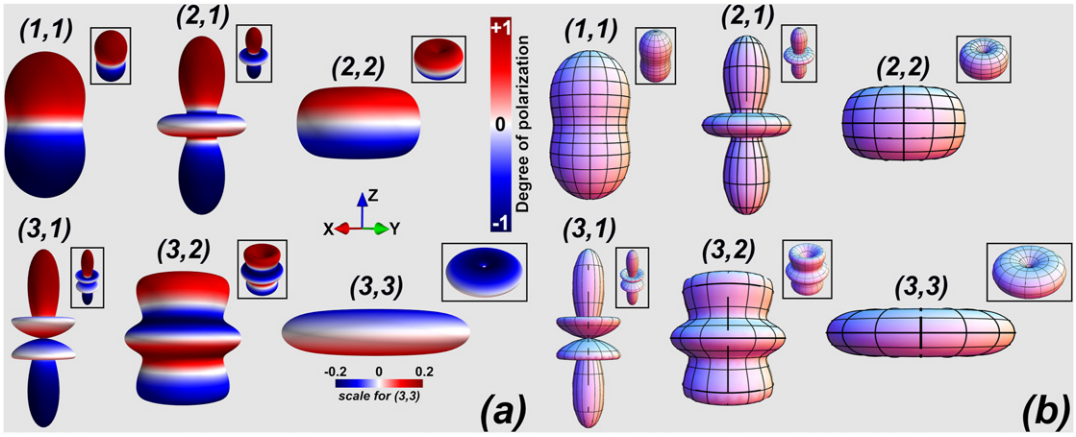

Figure 2. (a) Ionization-polarization surfaces for photoelectrons generated by a spherical wave of 5 MeV magnetic photons, with angular momentum (j, m) as labeled, irradiating Xe^{53+}. The ionization rate is measured by the distance from the origin to a point on the surface. The degree of polarization is indicated by the red-blue colormap. Note: surfaces with m a negative integer are obtained from those shown by flipping about the horizontal symmetry axes, and the $(3, 3)$ surface is plotted on a narrower color scale. (b) Isosurfaces of the Stokes parameter S_0 for the incident magnetic photon, obtained analytically. The upper insets are isometric views of each surface.

requirement, having a normalized ionization potential $I/m \approx 0.081$. The strong scaling of the ionization rate with atomic number Z (equation (14)) is a consideration in applications.

The degree of polarization is plotted in figure 2(a) for 5 MeV x-ray photons, satisfying the requirement $\omega \gg I$ of the analysis by a wide margin. The plots cover the range $j = 1, 2, 3$ for total angular momentum of the magnetic x-ray photons, and the appropriate components $m > 0$ thereof. The corresponding $m < 0$ plots are obtained by flipping about the horizontal symmetry axes.

For $m = \pm 1$, the surfaces of constant Stokes parameter S_0 (defined in equation (9)) have z as the symmetry axis. The magnetic photons with $m = 0$ produce isotropically unpolarized photoelectrons, as verified numerically, and so are omitted from the presented data. It should be pointed out that the shapes of the ionization-polarization surfaces in figure 2(a) can obscure the dependence of the degree of polarization on the electron polar angle of emission. For instance, one must look closely to see that for the case of irradiation by the $(j, m) = (3, 3)$ mode, there is a reversal in the sign of the polarization as one moves away from the north pole, beginning near $\theta_p \sim \pi/4$. To clarify this, lineouts obtained from figure 2(a) are provided in figure 3. Notice that there is a qualitative difference between the plots for $(1, 1)$ and $(2, 2)$ on the one hand and that for $(3, 3)$ on the other. In the former two there is a monotonic change in the degree of polarization over the range $0 \leqslant \theta_p \leqslant \pi$, whilst in the latter case there is a noticeable modulation of the degree of polarization. These differences in behavior are dictated by the detailed spatial variation of the photon wavefunction and those of the electron current, which are captured by the integrand of the S-matrix element. By explicitly working out a few numerical examples it has been verified that the depth and number of these modulations are not universal, but change considerably with the ionization potential of the atom and the photon energy, amongst others.

Figure 4 shows the variation of the differential ionization rate $\mathrm{d}w_{jm}/\mathrm{d}\varepsilon$ (equation (10)) versus photoelectron speed $\beta = \sqrt{1 - (m/\varepsilon)^2}$ for a broadband source of photons with energy in the range 5–105 MeV. The rate has a sharp fall-off as the photoelectron speed approaches the speed of light. Included is a plot for ionization of U^{91+} with the same photon parameters. In this case the normalized ionization potential $I/m \approx 0.2589$ marginally satisfies the $Z\alpha < 1$ requirement of the analysis (see reference [59]), whilst highlighting the strong scaling with Z.

4. Discussion

It must be emphasized that considering magnetic photons with a single (j, m)-pair is a simplification. In this paper the ideal case of a single class of magnetic photons is used to highlight the underlying physics and the interesting points that this novel irradiation approach exemplifies. It is likely that interference amongst modes will affect the degree of polarization. In practice, depending on the distribution of charge, current, and magnetization densities at the source, there will be a combination of Ej and Mj multipoles, with a range of (j, m)-pairs, that irradiates the atom [2]. This is determined by the experimental set up as well as the propagation to the target, and each case requires independent numerical evaluation. A more detailed study

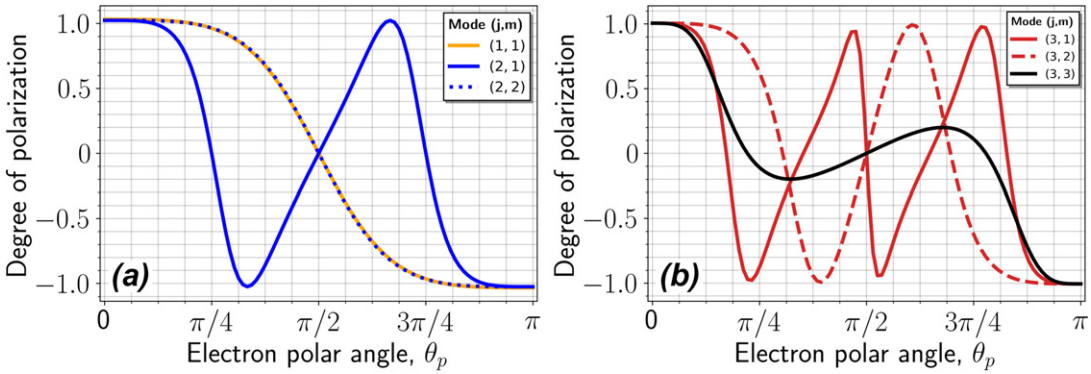

Figure 3. Degree of polarization of photoelectrons emerging from Xe^{53+} versus the polar angle for the case of irradiation with 5 MeV magnetic photon with total angular momentum (a) $j = 1, 2$ and (b) $j = 3$, and all positive azimuthal projections m thereof. The polarization is azimuthally-invariant, and has the opposite sign for $m < 0$.

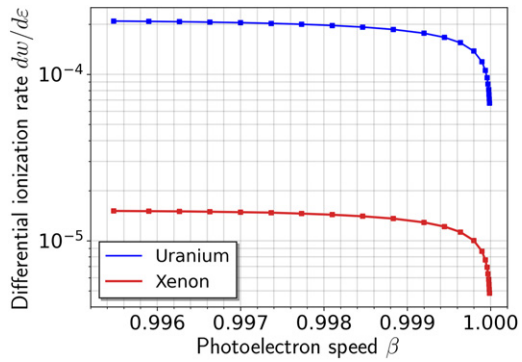

Figure 4. Differential ionization rate vs photoelectron speed β obtained by varying the photon energy in the range 5–105 MeV. Photoionization is effected by magnetic photons with total angular momentum $j = 1$ and component $m = +1$ thereof irradiating a Xe^{53+} ion. Also shown is the plot for irradiation of U^{91+}. Solid squares are from numerical evaluation of the integrand in equation (14) and the continuous curve is to guide the eye.

will no doubt address 'nonideal' effects, such as multimode irradiation, which may not necessarily be deleterious. For example, it has been shown that interference of the ionization paths in the presence of a photoionizing laser field and its second harmonic leads to the possibility of coherent control of the spin of the photoelectron [62, 63].

In the configuration considered, the photon energy must be high in order to obtain high energy photoelectrons. As a result, the precision needed to arrange a centro-symmetric system is onerous, since the tolerance is approximately the radiation wavelength. One would like to increase the wavelength, while maintaining photoelectron energy. This may be possible by transitioning to the tunneling regime, i.e. by increasing the irradiance with the wavelength. Analysis of this configuration would require a new effort, but some of the techniques employed here would likely be relevant.

Besides photoionization, spherical waves may be used in other processes to generate polarized leptons; e.g. a variant of the Bethe–Heitler process for generation of polarized electron–positron pairs. This, along with limitations of the analysis, are briefly considered in supplementary section 4.

5. Conclusion

In the majority of previous analyses, laser beams—typically linearly- or circularly-polarized and specified by the wavevector—have been employed to control the polarization of reaction byproducts. But photons can equally well be specified by their angular momentum. This is a natural approach for describing spherical waves of photons belonging to the class of fully structured light. The state of polarization of these photons varies with position on the associated Poincaré sphere, and all of these photon states contribute simultaneously to the helicity and directionality of photoionized electrons. An important consequence is that for a given initial angular momentum state (j, m) photoelectrons with both helicities are obtained and

their angular distribution is such that the opposite helicities can be extracted and employed in collider experiments with precise timing.

Acknowledgments

This work was supported by NRL 6.1 Base Funds and by DoE.

Data availability statement

All data that support the findings of this study are included within the article (and any supplementary files).

Author contributions

DFG proposed the concept, BH carried out the analysis, and DY performed the computations and created the figures based on discussions with DFG & BH. All contributed to the writing of the manuscript.

Additional information/ethical statement

The data and computation codes that support the findings of this study are available from DY upon request. The authors declare no competing interests.

ORCID iDs

B Hafizi https://orcid.org/0000-0003-3627-599X
D Younis https://orcid.org/0000-0002-5254-5905
D F Gordon https://orcid.org/0000-0003-0844-8988

References

[1] Moortgat-Pick G *et al* 2008 *Phys. Rep.* **460** 131
[2] Jackson J D 1975 *Classical Electrodynamics* 2nd edn (New York: Wiley)
[3] Zhan Q 2009 *Adv. Opt. Photon.* **1** 1
[4] Hancock S W, Zahedpour S and Milchberg H M 2021 *Phys. Rev. Lett.* **127** 193901
[5] Brown L S and Kibble T W B 1964 *Phys. Rev.* **133** A705
[6] Sarachik E S and Schappert G T 1970 *Phys. Rev.* D **1** 2738
[7] Olsen H and Maximon L C 1959 *Phys. Rev.* **114** 887
[8] Pratt R H 1961 *Phys. Rev.* **123** 1508
[9] Fano U 1969 *Phys. Rev.* **178** 131
[10] Sokolov A A and Ternov I M 1986 *Radiation from Relativistic Electrons* (New York: American Institute of Physics)
[11] Tsai Y S 1993 *Phys. Rev.* D **48** 96
[12] Okugi T *et al* 1996 *Japan. J. Appl. Phys.* **35** 3677
[13] Kirseborn K, Mikkelsen U, Uggerhøj E, Elsener K, Ballestrero S, Sona P and Vilakazi Z Z 2001 *Phys. Rev. Lett.* **87** 054801
[14] Ivanov D Y, Kotkin G L and Serbo V G 2005 *Eur. Phys. J.* C **40** 27
[15] Omori T *et al* 2006 *Phys. Rev. Lett.* **96** 114801
[16] Di Piazza A, Milstein A I and Müller C 2010 *Phys. Rev.* A **82** 062110
[17] Müller T-O and Müller C 2012 *Phys. Rev.* A **86** 022109
[18] Wöllert A, Bauke H and Keitel C H 2015 *Phys. Rev.* D **91** 125026
[19] Liu M M, Shao Y, Han M, Ge P, Deng Y, Wu C, Gong Q and Liu Y 2018 *Phys. Rev. Lett.* **120** 043201
[20] Chen Y Y, He P L, Shaisultanov R, Hatsagortsyan K Z and Keitel C H 2019 *Phys. Rev. Lett.* **123** 174801
[21] Wistisen T N 2020 *Phys. Rev.* D **101** 076017
[22] Li Y F, Chen Y Y, Wang W-M and Hu H S 2020 *Phys. Rev. Lett.* **125** 044802
[23] Matula O, Hayrapetyan A G, Serbo V G, Surzhykov A and Fritzsche S 2013 *J. Phys. B: At. Mol. Opt. Phys.* **46** 205002
[24] Scholz-Marggraf H M, Fritzsche S, Serbo V G, Afanasev A and Surzhykov A 2014 *Phys. Rev.* A **90** 013425
[25] Surzhykov A, Seipt D, Serbo V G and Fritzsche S 2015 *Phys. Rev.* A **91** 013403
[26] Surzhykov A, Seipt D and Fritzsche S 2016 *Phys. Rev.* A **94** 033420
[27] Müller R A, Seipt D, Beerwerth R, Ornigotti M, Szameit A, Fritzsche S and Surzhykov A 2016 *Phys. Rev.* A **94** 041402
[28] Hafizi B and Sprangle P 1991 *J. Opt. Soc. Am.* A **8** 705
[29] Solyanik-Gorgone M and Afanasev A 2019 *Phys. Rev.* B **99** 035204
[30] Lambropoulos P 1973 *Phys. Rev. Lett.* **30** 413
[31] Trabert D *et al* 2018 *Phys. Rev. Lett.* **120** 043202
[32] Nie Z *et al* 2021 *Phys. Rev. Lett.* **126** 054801
[33] Berestetskiĭ V B, Lifshitz E M and Pitaevskiĭ L P 2008 *Quantum Electrodynamics* 2nd edn (Oxford: Heinemann)

[34] Stratton J A 1941 *Electromagnetic Theory* (New York: McGraw-Hill)
[35] Bjorken J D and Drell S D 1964 *Relativistic Quantum Mechanics* (New York: McGraw-Hill)
[36] Bjorken J D and Drell S D 1965 *Relativistic Quantum Fields* (New York: McGraw-Hill)
[37] Bula C *et al* 1996 *Phys. Rev. Lett.* **76** 3116
[38] Burke D L *et al* 1997 *Phys. Rev. Lett.* **79** 1626
[39] Bamber C *et al* 1999 *Phys. Rev.* D **60** 092004
[40] Boca M and Florescu V 2009 *Phys. Rev.* A **80** 053403
[41] Krajewska K and Kamiński J Z 2012 *Phys. Rev.* A **86** 052104
[42] Mackenroth F and Di Piazza A 2013 *Phys. Rev. Lett.* **110** 070402
[43] Lezhnin K V, Sasorov P V, Korn G and Bulanov S V 2018 *Phys. Plasmas* **25** 123105
[44] Stark D J, Toncian T and Arefiev A V 2016 *Phys. Rev. Lett.* **116** 185003
[45] Jansen O, Wang T, Stark D J, d'Humières E, Toncian T and Arefiev A V 2018 *Plasma Phys. Control. Fusion* **60** 054006
[46] Wang T, Ribeyre X, Gong Z, Jansen O, d'Humiéres E, Stutman D, Toncian T and Arefiev A 2020 *Phys. Rev. Appl.* **13** 054024
[47] Younis A H, Davidson A, Hafizi B and Gordon D F 2020 Diagnostic techniques for particle-in-cell simulations of laser-produced gamma-rays in the strong-field QED regime *Proc. Advanced Accelerator Concepts Seminar Series* NRL-MR6791–20-10,122
[48] Younis D, Hafizi B and Gordon D F 2022 Generation of collimated vortex gamma-rays from intense Poincaré beam-plasma interaction *Phys. Plasmas* **29** 093106
[49] Allen L, Beijersbergen M W, Spreeuw R J C and Woerdman J P 1992 *Phys. Rev.* A **45** 8185
[50] Padgett M J and Courtial J 1999 *Opt. Lett.* **24** 430
[51] Padgett M J and Allen L 2000 *Contemp. Phys.* **41** 275
[52] Holleczek A, Aiello A, Gabriel C, Marquardt C and Leuchs G 2011 *Opt. Express* **19** 9714
[53] Milione G, Sztul H I, Nolan D A and Alfano R R 2011 *Phys. Rev. Lett.* **107** 053601
[54] Barnett S M, Allen L, Cameron R P, Gilson C R, Padgett M J, Speirits F C and Yao A M 2016 *J. Opt.* **18** 064004
[55] Morgan J, Hemsing E, McNeil B W J and Yao A 2020 *New J. Phys.* **22** 072001
[56] Forbes A, de Oliveira M and Dennis M R 2021 *Nat. Photon.* **15** 253
[57] Naidoo D, Roux F S, Dudley A, Litvin I, Piccirillo B, Marrucci L and Forbes A 2016 *Nat. Photon.* **10** 327
[58] Halzen F and Martin A D 1984 *Quarks & Leptons* (New York: Wiley)
[59] Klaiber M, Yakaboylu E and Hatsagortsyan K Z 2013 *Phys. Rev.* A **87** 023418
[60] Hafizi B, Gordon D F and Palastro J P 2017 *Phys. Rev. Lett.* **118** 133201
[61] Hafizi B, Gordon D F and Kaganovich D 2019 *Phys. Rev. Lett.* **122** 233201
[62] Gryzlova E V, Popova M M and Grum-Grzhimailo A N 2020 *Phys. Rev.* A **102** 053116
[63] Scholak T and Brumer P 2014 *J. Chem. Phys.* **141** 204311